Imaging signatures of meningioma and low-grade glioma: a diffusion tensor, magnetization transfer and quantitative longitudinal relaxation time MRI study

Rory J. Piper[1], Shadia Mikhael[2], Joanna M. Wardlaw[1,2,3], David H. Laidlaw[4], Ian R. Whittle[1,3] and Mark E. Bastin[1,2,3].

[1]College of Medicine and Veterinary Medicine, University of Edinburgh, UK.
[2]Brain Research Imaging Centre, University of Edinburgh, UK.
[3]Centre for Clinical Brain Sciences, University of Edinburgh, UK.
[4]Computer Science Department, Brown University, Providence, RI, United States.

Corresponding author: Rory J. Piper; R.J.Piper@sms.ed.ac.uk; College of Medicine and Veterinary Medicine, University of Edinburgh, UK; 49 Little France Crescent, Edinburgh, EH16 4SB.

11th December 2015

This work has been presented at the International Society for Magnetic Resonance Imaging in Medicine (ISMRM) British Chapter 20th Annual Scientific Meeting, September, September 4-5, 2014; Edinburgh, UK.

Abstract

Differentiation of cerebral tumor pathology currently relies on interpretation of conventional structural MRI and in some cases histology. However, more advanced MRI methods may provide further insight into the organization of cerebral tumors and have the potential to aid diagnosis. The objective of this study was to use multimodal quantitative MRI to measure the imaging signatures of meningioma and low-grade glioma (LGG). Nine adults with meningioma and 11 with LGG were identified, and underwent standard structural, quantitative longitudinal relaxation time (T_1) mapping, magnetization transfer and diffusion tensor MRI. Maps of mean ($\langle D \rangle$), axial (λ_{AX}) and radial (λ_{RAD}) diffusivity, fractional anisotropy (FA), magnetization transfer ratio (MTR) and T_1 were generated on a voxel-by-voxel basis. Using structural and echo-planar T_2-weighted MRI, manual region-of-interest segmentation of brain tumor, edema, ipsilateral and contralateral normal-appearing white matter (NAWM) was performed. Differences in imaging signatures between the different tissue types, both absolute mean values and ratios relative to contralateral NAWM, were assessed using t-tests with statistical significance set at $p < 0.05$. For both absolute mean values and ratios relative to contralateral NAWM, there were significant differences in $\langle D \rangle$, λ_{AX}, λ_{RAD}, FA, MTR and T_1 between meningioma and LGG tumor tissue, respectively. Only T_1 and FA differed significantly between edematous tissue associated with the two tumor types. These results suggest that multimodal MRI biomarkers are significantly different, particularly in tumor tissue, between meningioma and LGG. By using quantitative multimodal MRI it may be possible to identify tumor pathology non-invasively.

Key words: low-grade glioma; meningioma; magnetic resonance imaging; diffusion; magnetization transfer; longitudinal relaxation time

1. Introduction

Cerebral tumors cause neurological symptoms by disturbing the architecture and water content of brain tissue (1). Gliomas, either low- (LGG; World Health Organisation (WHO) grades I-II) or high-grade (HGG; WHO grades III-IV), are malignant, intrinsic cerebral tumors that may cause tumor-infiltrative edema. Meningiomas are mostly benign, extrinsic cerebral tumors that do not infiltrate surrounding parenchyma. Mengingiomas may give rise to vasogenic edema in the peritumoral tissue (2); however, in both glioma and meningioma, edema is not always present.

In a minority of cases, the radiological diagnosis of cerebral tumors may be insufficient on conventional structural imaging, e.g. T2-weighted (T2W) MRI, with or without contrast, and confident diagnosis must rely on histopathological analysis (3). Unfortunately, the invasive acquisition of tumor biopsy is not without risk. Therefore, the development of reliable neuroradiological techniques to predict tumor pathology is required to identify cerebral tumors and inform intervention. As a first step towards this goal, a number of studies have identified the diffusion tensor MRI (DT-MRI) signatures of HGG and meningiomas (4–6). However, there is still a need to report the imaging signatures of other tumor pathologies such as LGG. Furthermore, there is a need to investigate whether other imaging modalities, such as magnetization transfer MRI (MT-MRI) and quantitative longitudinal relaxation time (T_1) mapping, can provide useful data to aid tumor characterization.

DT-MRI is a non-invasive imaging technique that measures the random motion of water molecules across the brain due to thermal energy (7). It provides two common biomarkers of tissue microstructure, mean diffusivity ($\langle D \rangle$), which measures the magnitude of water molecule diffusion, and fractional anisotropy (FA), which measures its directional coherence. Low $\langle D \rangle$ and high FA values imply good microstructural integrity and organization of tissue, especially in cerebral white matter, while high $\langle D \rangle$ and low FA values may indicate compromised cellular structure (8). Two further biomarkers provided by DT-MRI include the axial (λ_{AX}) and radial (λ_{RAD}) diffusivities which represent water diffusion parallel and perpendicular to the axonal fibers and may be used to infer axonal and/or myelin injury (9).

MT-MRI provides a further metric of white matter integrity, the magnetization transfer ratio (MTR). This parameter measures the efficiency of the magnetization exchange between the relatively free water protons inside tissue and those bound to protein macromolecules in cellular membranes. Any pathological change in cell membrane macromolecules resulting

from loss of tissue structure, such as the presence of edema, will cause a reduction in MTR (10).

T_1-mapping may also have use in identifying abnormalities in brain structure caused by cerebral neoplasms. This is due to the observation that a linear relationship exists between the inverse brain water content and the longitudinal relaxation rate ($1/T_1$) in human brain (11). These findings suggest that the longitudinal signal decay of brain tissue, which is observed to be a single exponential, arises from a fast exchange between free and hydration water compartments (12). Thus, the measured T_1 time is a weighted average of the free (long T_1) and bound (short T_1) water phases (13). Quantitative maps of T_1 may therefore provide valuable information on the spatial distribution of brain water abnormalities associated with intracranial tumors (4).

A recent study by De Belder et al. compared meningioma (N = 20) and HGG (N = 15) using DT-MRI (5). These investigators found that FA values were significantly higher and <D> values significantly lower for meningioma and associated edema than for HGG, indicating the higher degree of cellular organization in meningioma compared with HGG. These findings are in agreement with those reported by Bastin et al. who found that FA values were significantly higher in meningioma (N = 3) than HGG (N = 3), while ⟨D⟩ values were significantly lower, findings that were repeated when comparing edema values between patient groups (4). In addition, this study revealed that T_1 values were significantly lower in meningioma compared with HGG indicating less disturbance in brain water homeostasis. A further study by Garcia et al. measured differences in MTR values between glioblastoma multiforme (N = 9) and meningioma (N = 4), with the former showing the most abnormal and the latter the least abnormal MTR values compared with normal-appearing tissue (6). These studies demonstrate the potential for quantitative imaging biomarkers to provide useful information about tumor properties, and possibly differentiate between different tumor types. However, in order to achieve this potential further data encompassing other tumor types is required.

The objective of the current study was to investigate whether multiple imaging biomarkers provided by DT-, MT- and T_1-mapping MRI were significantly different in meningioma compared with LGG using region-of-interest (ROI) analysis. Due to the differences in pathology between these two tumor types, we hypothesized that each biomarker would indicate a higher microstructural integrity in meningioma compared with LGG for tumor, edema and ipsilateral white matter compared with contralateral normal-appearing white matter (NAWM).

2. Materials and Methods

2.1 Subjects

Nine patients with meningioma (5 male; mean age 49.8 ± 10.5 (range 35 – 64) years) and 11 with LGG (5 male; mean age 49.1 ± 11.7 (range 30 – 63) years) were identified by clinical and radiological assessment with subsequent confirmation of tumor type by histology. None of these subjects had begun corticosteroid treatment, radiotherapy or chemotherapy at the time of MRI, and there was no evidence of neurological disorders other than the primary neoplasm from the radiological data. The local ethics committee approved the study and informed consent was obtained from each patient.

2.2 MRI acquisition

All MRI data were obtained using a GE Signa Horizon HDxt 1.5 T clinical scanner (General Electric, Milwaukee, WI, USA) using a self-shielding gradient set with maximum gradient strength of 33 mT/m, and an 8-channel phased-array head coil. The examination comprised the following whole brain sequences acquired with contiguous axial slice locations: standard structural T2W MRI, two T_1-weighted fast-spoiled gradient echo (FSPGR) scans with 2 and 12° flip angles for quantitative T_1-mapping, two standard spin echo sequences acquired with and without a magnetization transfer pulse applied 1 kHz from the water resonance frequency for MT-MRI, and finally a DT-MRI protocol consisting of seven T2W and sets of diffusion-weighted ($b = 1000$ s/mm^2) single-shot spin-echo echo-planar imaging (EPI) volumes acquired with diffusion gradients applied in 64 non-collinear directions (14). The acquisition took approximately 50 minutes. The acquisition parameters for the structural T2W, DT-, MT- and T_1-mapping MRI protocols, i.e. field-of-view (256 × 256 mm in all cases), imaging matrix (128 × 128 for DT-MRI, and 256 × 256 for the other sequences), slice thickness and location (72 × 2 mm in all cases), were chosen to allow easier co-registration between scans so that the imaging biomarkers could be accurately measured within ROI in the EPI and non-EPI based sequences.

2.3 Image processing

MRI data were converted from DICOM (http://dicom.nema.org) to NIfTI-1 (http://nifti.nimh.nih.gov/nifti-1) format, and pre-processed using FSL tools (http://www.fmrib.ox.ac.uk/fsl). The DT-MRI data were pre-processed to extract the brain (15), and remove bulk patient motion and eddy current induced artifacts by registering the diffusion-weighted to the first T2W EPI volume for each subject (16). From these MRI data, $\langle D \rangle$, λ_{AX}, λ_{RAD} and FA volumes were generated for every subject using DTIFIT.

Quantitative maps of T_1 were obtained by registering the 2 and 12° FSPGR sequences to the T2W structural scan using FLIRT, with T_1 being determined from

$$\frac{1}{T_1} = \frac{1}{TR} \ln\left[\frac{S_R \sin\alpha_2 \cos\alpha_1 - \sin\alpha_1 \cos\alpha_2}{S_R \sin\alpha_2 - \sin\alpha_1}\right], \quad (1)$$

where TR is the repetition time (= 6 ms), $\alpha_1 = 2°$, $\alpha_2 = 12°$, $S_R = S_1 / S_2$, and S_1 and S_2 the signal intensity values in each voxel for α_1 and α_2 respectively (17). Similarly maps of MTR were obtained by registering the two component spin echo sequences to the T2W structural volume and calculating this biomarker on a voxel-by-voxel basis using

$$\text{MTR} = 100\frac{M_0 - M_s}{M_0}, \quad (2)$$

where M_s and M_0 represent signal intensities with and without the magnetization transfer pulse (10).

Using Analyze11.0™ software (Mayo Clinic, KS, USA; http://www.analyzedirect.com) and the standard structural and EPI-based T2W sequences, one investigator (RJP) conducted manual ROI segmentation of brain tumor and edema in each patient. Firstly, ROI were carefully drawn round tumor and edema in each slice where they were visible on the structural T2W scan. These regions were then masked off, and FSL's FAST (18) applied to identify regions of NAWM in the ipsi- and contralateral hemispheres. To provide measurements of the imaging biomarkers in the different tissue types, these masks were then applied directly to the MTR and T_1 volumes without further registration steps, and to the $\langle D \rangle$, FA, λ_{AX} and λ_{RAD} volumes by applying the non-linear warp field obtained by non-linear registration (FSL's FNIRT) of the structural T2W volume to the DT-MRI T2W EPI volume.

2.4 Statistics

In addition to presenting mean values of $\langle D \rangle$, FA, λ_{AX}, λ_{RAD}, MTR and T_1 in each tissue type, each imaging biomarker measurement was normalized by the corresponding NAWM values in the contralateral hemisphere, i.e. tumor/contralateral NAWM, edema/contralateral NAWM and ipsilateral NAWM/contralateral NAWM, to allow each patient to act as their own control. T-tests were then used to compare these mean and ratio values between meningioma and LGG in the various tissue types. Statistical analyses were carried out using GraphPadPrism v5.0 (GraphPad Software Inc, CA, USA; http://www.graphpad.com) for MacOSX. Statistical significance was set at $p < 0.05$, with all data presented as mean ± SD (range).

3. Results

Six patients with meningioma and six with LGG had edema present on structural T2W MRI; two patients with LGG were excluded since tumor could not be sufficiently delineated from surrounding edema.

Figures 1 and 2 show examples of ROI segmentations and biomarker maps for two representative patients with meningioma and LGG. For both tumor types, note the reduced MTR and FA, and elevated T_1, $\langle D \rangle$, λ_{AX} and λ_{RAD} in tumor and edema compared with surrounding normal-appearing tissue.

3.1 Mean imaging biomarker values

Table 1 shows mean values for all imaging biomarkers in tumor, edema, ipsi- and contralateral white matter. For tumor tissue, meningioma had higher MTR (43.67 ± 3.28 (range 37.77 – 47.93) versus 39.02 ± 4.04 (range 32.29 – 43.43) %; $p < 0.02$) and FA (0.19 ± 0.04 (range 0.12 – 0.25) versus 0.11 ± 0.02 (range 0.08 – 0.16); $p << 0.001$) values than LGG, and significantly lower values of T_1 (1.62 ± 0.13 (range 1.40 – 1.82) versus 2.01 ± 0.45 (range 1.56 – 2.84) s; $p = 0.02$), $\langle D \rangle$ (856 ± 130 (range 553 – 969) versus 1367 ± 168 (range 1179 – 1687) × 10^{-6} mm^2/s; $p << 0.001$), λ_{AX} (1006 ± 149 (range 677 – 1151) versus 1511 ± 166 (range 1305 – 1816) × 10^{-6} mm^2/s; $p << 0.001$) and λ_{RAD} (781 ± 123 (range 491 – 878) versus 1294 ± 171 (range 1116 – 1623) × 10^{-6} mm^2/s; $p << 0.001$). For edematous brain, there were no significant differences in MTR, $\langle D \rangle$, λ_{AX} and λ_{RAD} between meningioma and LGG. However, differences in T_1 (1.31 ± 0.19 (range 1.08 – 1.56) versus 1.68 ± 0.35 (range 1.31 – 2.23) s; $p < 0.05$) and FA (0.24 ± 0.05 (range 0.20 – 0.33) versus 0.15 ± 0.02 (range 0.12 – 0.17); $p < 0.002$) were significant. For both ipsi- and contralateral white matter, there was no significant difference in any imaging biomarker between tumor pathologies.

3.2 Imaging biomarker values relative to contralateral normal-appearing white matter

The ratios for all imaging biomarker measurements in tumor, edema and ipsilateral NAWM relative to contralateral NAWM are summarized in Table 2 and Figure 3. Meningioma MTR was significantly higher than that of LGG for tumor (0.79 ± 0.05 (range 0.72 – 0.86) versus 0.69 ± 0.07 (range 0.58 – 0.76); $p = 0.002$), but not for edema or ipsilateral white matter. Meningioma T_1 was significantly lower than that of LGG for both tumor (1.61 ± 0.12 (range 1.38 – 1.78) versus 1.91 ± 0.40 (range 1.57 – 2.89); $p < 0.05$) and edema (1.36 ± 0.22 (range 1.01 – 1.63) versus 1.62 ± 0.37 (range 1.26 – 2.27); $p << 0.001$). Ipsilateral white matter

showed no significant difference in either MTR or T_1 relative to contralateral NAWM between tumor pathologies.

For tumor tissue, $\langle D \rangle$ (1.22 ± 0.18 (range 0.79 – 1.38) versus 1.92 ± 0.31 (range 1.48 – 2.41); $p << 0.001$), λ_{AX} (1.12 ± 0.17 (range 0.74 – 1.27) versus 1.67 ± 0.23 (range 1.36 – 2.06); $p << 0.001$) and λ_{RAD} (1.29 ± 0.21 (range 0.84 – 1.55) versus 2.10 ± 0.37 (range 1.57 – 2.66); $p << 0.001$) were all significantly lower in meningioma than LGG. FA was significantly higher in meningioma compared with LGG (0.71 ± 0.19 (range 0.36 – 0.94) versus 0.43 ± 0.11 (range 0.31 – 0.61); $p < 0.002$) in tumor tissue. Edema ratios were not significantly different except for FA where meningioma was significantly higher than LGG (0.90 ± 0.31 (range 0.60 – 1.49) versus 0.58 ± 0.09 (range 0.49 – 0.72); $p < 0.05$). Ipsilateral white matter showed no significant difference in any water diffusion parameter relative to contralateral NAWM between tumor pathologies.

4. Discussion

We employed multiple DT-, MT- and T_1-mapping MRI biomarkers to characterize differences in imaging signatures between tumor, edema, and ipsilateral and contralateral white matter in patients with meningioma and LGG. In summary, we found significant differences in each parameter between meningioma and LGG tumor tissue, with the former having values closer to contralateral NAWM, suggesting that the organization of tissue is greater in meningioma than LGG. However, only T_1 and FA ratios differed significantly between edema found in subjects with meningioma and LGG, both of which indicate a higher organization of tissue in the edema of meningioma. However, the small sample size of our study (N = 6 for both groups) may have resulted in failure to detect significant differences in the other biomarkers in edematous tissue. No differences were detected in any parameters in the ipsilateral white matter between meningioma and LGG. No parameter identified a difference between ipsilateral and contralateral NAWM in either tumor pathology.

Our findings demonstrate that these multimodal MRI biomarkers differ significantly between meningioma and LGG in tumor tissue. Although these tumors are not often mistaken for one another on conventional diagnostic imaging (e.g. T2W MRI), our study supports the idea put forward by other investigators that imaging signatures may allow objective prediction of pathology (5,19). Mean T_1 values were significantly higher and FA values were significantly lower in the edema of LGG compared to that of meningioma, suggesting a greater disruption of surrounding white matter architecture. This finding is in concordance with the infiltrative nature of glioma edema, such that the actual tumor margin is often found microscopically

beyond that observed on structural T2W MRI (19). Meningiomas are instead postulated to displace surrounding white matter tracts and tend to give rise to 'pure vasogenic' edema.

Given differences in patient populations and acquisition protocols, our results are generally concordant with similar studies that have measured differences between quantitative imaging biomarkers in cerebral tumors. For meningioma, our mean ⟨D⟩ values for tumor (856 ± 130 × 10^{-6} mm^2/s) and edema (1146 ± 152 × 10^{-6} mm^2/s) are close to those reported by Bastin et al. (907 ± 92 and 1316 ± 191 × 10^{-6} mm^2/s respectively) (4). Similarly, our mean FA values for meningioma (0.19 ± 0.04) and associated edema (0.24 ± 0.05) are close to those reported by De Belder et al. (0.27 ± 0.07 and 0.18 ± 0.12 respectively) (5) and Bastin et al. (0.22 ± 0.06 and 0.22 ± 0.07 respectively) (4). For T_1, our mean values for meningioma (1.62 ± 0.13 s) and edema (1.31 ± 0.19 s) are also fairly close to those in Bastin et al. (1.29 ± 0.08 and 1.21 ± 0.14 s respectively). For LGG, De Belder et al. report FA values in HGG (0.17 ± 0.04) that are slightly higher than those we find in LGG (0.11 ± 0.02), which does not fit with the hypothesis that as glioma grade increases so does the disruption to cellular organization. Conversely for edematous brain, our FA values for LGG (0.15 ± 0.02) are higher than those reported by De Belder et al. for HGG (0.12 ± 0.04) which does agree with LGG producing a more marked effect on surrounding tissue.

In addition to DT-, MT- and T_1-mapping MRI, there are several other MR modalities that provide biomarkers that are useful in characterizing meningioma and glioma. For example, dynamic contrast-enhanced (DCE) and dynamic susceptibility contrast (DSC) MRI provide metrics of tissue permeability and perfusion that can describe the different vascular properties of these two common tumor types, their grade, response to treatment and prognosis (17,20-23). Meningiomas are often highly vascular without a blood-brain barrier, while gliomas have varying degrees of vascularity and blood-brain barrier disruption depending on grade, characteristics that can potentially allow their differentiation (20). Proton MR spectroscopy (^{1}H-MRS), both long and short echo time, has also been used to characterize tumor type and provide insights into tumor metabolism; see Horská and Barker (24) for a review. ^{1}H-MRS findings in cerebral tumors typically show reduced N-acetylaspartate and creatine, and elevated choline. However, one study also found that 21 of 23 meningiomas imaged had elevated alanine signals (1.5 T), regardless of typical or atypical type (25), while another reported that 17 meningioma cases showed a peak at 3.8 ppm (3 T), perhaps corresponding to glutamate, that was not evident in either 24 HGG or nine metastasis cases (26).

A limitation of our study, beyond the small sample size, was the difficulty encountered with manual segmentation of the cerebral tumors. This problem was particularly pronounced in

LGG where the demarcation of tumor, edema and parenchyma was sometimes unclear and therefore subjective on ROI measurement. (MRI Intravenous contrast agents often aid differentiation of the different tissue types, but was not used here due to ethical considerations.) Performing the study at higher field strength (3T) may have helped reduce this problem (27). Additionally we were not able to compare our segmentation margins directly to pathology, as performed in another study (28). A number of methods have been designed to enable automatic or semi-automatic segmentation of brain tumors. For example, Kaus et al., report a method using gradient-echo MRI that allows automated segmentation of meningioma and LGG which is faster than manual segmentation (5-10 minutes versus 3-5 hours) and more reproducible between users (29). However, while this and similar automatic methods may provide rapid and reproducible segmentations, the results may still not be accurate with regard to the underlying pathology.

We were not able to identify differences in any biomarker in the ipsilateral white matter between meningioma and LGG suggestive of increased tumor infiltration in the latter. However, our method may not have been sensitive enough to measure such differences given that we measured the average value for the entire hemisphere in which the tumor was present. A more sensitive approach may have been achieved by using standardized ROI placement closer to the tumor margin. However, a study by Price et al. used smaller ROI to measure 'local' ipsilateral white matter structure and did not report a significant difference between this value and contralateral NAWM in cases of non-HGG and meningioma (30).

Another limitation of our work is that we have not separately analyzed the subtypes of meningioma or LGG. Previous work has shown an inverse correlation between $\langle D \rangle$ and the grade of astrocytic tumors (31), while the range of FA values are greater in HGG than LGG (32). In addition, both diffusion-weighted and DT-MRI have been employed to show differences in diffusion measurements between meningioma of different histopathology (33,34).

Finally, T_1 values were measured using a clinically optimized two flip angle method, also known as 'DESPOT1' (17,35). This approach has the advantage of generating T_1 maps with whole-brain coverage and adequate signal-to-noise ratio within a short acquisition time. However, the resulting T_1 values tend to be larger than those obtained using standard inversion recovery methods (36), while flip angle variations across the brain caused by radiofrequency field inhomogeneities also introduce errors. At 1.5 T and using a radiofrequency transmit volume coil, such flip angle variations should be minimized and be reasonably consistent within the cohort.

From our study findings and limitations, a number of recommendations for further research can be made. Firstly, it may be suggested that using a combination of multimodal structural- and water diffusion tensor-based biomarkers may allow quantitative and perhaps computer-automated distinction between tumors of different pathology. Other investigators have suggested that a radiological method may even be able to replace invasive biopsy in the diagnosis of brain tumors. For example, a study by Byrnes et al. measured ⟨D⟩ and FA in tumor and edema and found that imaging profiles alone were able to identify correctly glioblastoma in 69%, meningioma in 75% and metastasis in 100% of cases (37). In another study, the same group was able to distinguish correctly glioblastoma (87.5%) and cerebral metastases (83.3%) using just ⟨D⟩ and FA parameters (38). However, these studies did not include other tumor types such as LGG. With these and our findings in mind, it may therefore be possible to devise a quantitative index of imaging signatures of cerebral tumors. Such an index may support non-invasive and accurate prediction of tumor pathology. Secondly, there is a need to develop accurate and reliable methods to segment cerebral tumors, either using manual or more sophisticated automated methods. Finally, much larger studies of a wide range of patients are now required to develop further the use of quantitative MRI in brain tumor research.

5. Conclusions

These results suggest that DT-, MT- and T_1-mapping MRI biomarkers are significantly different between edema, and in particular tumor tissue, in meningioma and LGG; ratios to contralateral NAWM show that the organization of tissue in the edema of meningioma is closer to normality than LGG. However, our results require validation in studies with larger samples. Nevertheless, by using multiple quantitative MRI biomarkers it may be possible to employ neuroimaging to characterize tumor pathology accurately and non-invasively.

Acknowledgements

All imaging was performed in the Brain Research Imaging Centre, University of Edinburgh (http://www.bric.ed.ac.uk), and was funded by NIH grant R01 EB004155-03. JMW is supported by the Scottish Funding Council through the SINAPSE Collaboration (http://www.sinapse.ac.uk).

References

1. Sinha S, Bastin ME, Whittle IR, Wardlaw JM. Diffusion tensor MR imaging of high-grade cerebral gliomas. AJNR Am J Neuroradiol 2002;23:520–7.
2. Ide M, Jimbo M, Kubo O, Yamamoto M, Imanaga H. Peritumoral brain edema associated with meningioma--histological study of the tumor margin and surrounding brain. Neurol Med Chir (Tokyo) 1992;32:65–71.
3. Kondziolka D, Lunsford L, Martinez A. Unreliability of contemporary neurodiagnostic imaging in evaluating suspected adult supratentorial (low-grade) astrocytoma. J Neurosurg 1993;79:533–6.
4. Bastin ME, Sinha S, Whittle IR, Wardlaw JM. Measurements of water diffusion and T1 values in peritumoural oedematous brain. Neuroreport 2002;13:1335–40.
5. De Belder FE, Oot AR, Van Hecke W, Venstermans C, Menovsky T, Van Marck V, Van Goethem J, Van den Hauwe L, Vandekerckhove M, Parizel PM. Diffusion tensor imaging provides an insight into the microstructure of meningiomas, high-grade gliomas, and peritumoral edema. J Comput Assist Tomogr 2012;36:577–82.
6. Garcia M, Gloor M, Bieri O, Radue E-W, Lieb JM, Cordier D, Stippich C. Imaging of Primary Brain Tumors and Metastases with Fast Quantitative 3-Dimensional Magnetization Transfer. J Neuroimaging 2015; In press.
7. Basser PJ, Mattiello J, LeBihan D. Estimation of the effective self-diffusion tensor from the NMR spin echo. J Magn Reson B 1994;103:247–54.
8. Basser PJ, Pierpaoli C. Microstructural and physiological features of tissues elucidated by quantitative-diffusion-tensor MRI. J Magn Reson B 1996;111:209–19.
9. Song S-K, Sun S-W, Ramsbottom MJ, Chang C, Russell J, Cross AH. Dysmyelination revealed through MRI as increased radial (but unchanged axial) diffusion of water. Neuroimage 2002;17:1429–36.
10. Silver NC, Barker GJ, MacManus DG, Tofts PS, Miller DH. Magnetisation transfer ratio of normal brain white matter: a normative database spanning four decades of life. J Neurol Neurosurg Psychiatry 1997;62:223–8.
11. Fatouros P, Marmarou A, Kraft K, Inao S, Schwarz F. In vivo brain water determination by T1 measurements: effect of total water content, hydration fraction, and field strength. Magn Reson Med 1991;17:402–13.
12. Fullerton GD, Potter JL, Dornbluth NC. NMR relaxation of protons in tissues and other macromolecular water solutions. Magn Reson Imaging 1982;1:209–26.

13. Naruse S, Horikawa Y, Tanaka C, Hirakawa K, Nishikawa H, Yoshizaki K. Significance of proton relaxation time measurement in brain edema, cerebral infarction and brain tumors. Magn Reson Imaging 1986;4:293–304.
14. Jones DK, Williams SCR, Gasston D, Horsfield MA, Simmons A, Howard R. Isotropic resolution diffusion tensor imaging with whole brain acquisition in a clinically acceptable time. Hum Brain Mapp 2002;15:216–30.
15. Smith SM. Fast robust automated brain extraction. Hum Brain Mapp 2002;17:143–55.
16. Jenkinson M, Smith S. A global optimisation method for robust affine registration of brain images. Med Image Anal 2001;5:143–56.
17. Armitage PA, Schwindack C, Bastin ME, Whittle IR. Quantitative assessment of intracranial tumor response to dexamethasone using diffusion, perfusion and permeability magnetic resonance imaging. Magn Reson Imaging 2007;25:303–10.
18. Zhang Y, Brady M, Smith S. Segmentation of brain MR images through a hidden Markov random field model and the expectation-maximization algorithm. IEEE Trans Med Imaging 2001;20:45–57.
19. Lee EJ, Ahn KJ, Lee EK, Lee YS, Kim DB. Potential role of advanced MRI techniques for the peritumoural region in differentiating glioblastoma multiforme and solitary metastatic lesions. Clin Radiol 2013;68:e689-97.
20. Cha S, Yang L, Johnson G, Lai A, Chen MH, Tihan T, Wendland M, Dillon WP. Comparison of microvascular permeability measurements, K(trans), determined with conventional steady-state T1-weighted and first-pass T2*-weighted MR imaging methods in gliomas and meningiomas. AJNR Am J Neuroradiol 2006;27:409-17.
21. Zhang N, Zhang L, Qiu B, Meng L, Wang X, Hou BL. Correlation of volume transfer coefficient Ktrans with histopathologic grades of gliomas. J Magn Reson Imaging 2012;36:355-63.
22. Mills SJ, Patankar TA, Haroon HA, Balériaux D, Swindell R, Jackson A. Do cerebral blood volume and contrast transfer coefficient predict prognosis in human glioma? AJNR Am J Neuroradiol 2006;27:853-8.
23. Skinner JT, Moots PL, Ayers GD, Quarles CC. On the use of DSC-MRI for measuring vascular permeability. AJNR Am J Neuroradiol 2015 Oct 1.
24. Horská A, Barker PB. Imaging of brain tumors: MR spectroscopy and metabolic imaging. Neuroimaging Clin N Am 2010;20:293-310.

25. Demir MK, Iplikcioglu AC, Dincer A, Arslan M, Sav A. Single voxel proton MR spectroscopy findings of typical and atypical intracranial meningiomas. Eur J Radiol 2006;60:48-55.
26. Kousi E, Tsougos I, Fountas K, Theodorou K, Tsolaki E, Fezoulidis I, Kapsalaki E. Distinct peak at 3.8 ppm observed by 3T MR spectroscopy in meningiomas, while nearly absent in high-grade gliomas and cerebral metastases. Mol Med Rep 2012;5:1011-8.
27. Alvarez-Linera J. 3 T MRI: Advances in brain imaging. Eur J Radiol 2008;67:415–26.
28. Price SJ, Jena R, Burnet NG, Hutchinson PJ, Dean AF, Peña A, Pickard JD, Carpenter TA, Gillard JH. Improved delineation of glioma margins and regions of infiltration with the use of diffusion tensor imaging: an image-guided biopsy study. AJNR Am J Neuroradiol 2006;27:1969–74.
29. Kaus M, Warfield S, Nabavi A, Black P, Jolesz F, Kikinis R. Automated segmentation of MR images of brain tumors. Radiology 2001;218:586–91.
30. Price SJ, Burnet NG, Donovan T, Green HAL, Peña A, Antoun NM, Pickard JD, Carpenter TA, Gillard JH. Diffusion tensor imaging of brain tumours at 3T: a potential tool for assessing white matter tract invasion? Clin Radiol 2003;58:455–62.
31. Yamasaki F, Kurisu K, Satoh K, Arita K, Sugiyama K, Ohtaki M, Takaba J, Tominaga A, Hanaya R, Yoshioka H, Hama S, Ito Y, Kajiwara Y, Yahara K, Saito T, Thohar MA. Apparent diffusion coefficient of human brain tumors at MR imaging. Radiology 2005;235:985–91.
32. White ML, Zhang Y, Yu F, Jaffar Kazmi SA. Diffusion tensor MR imaging of cerebral gliomas: evaluating fractional anisotropy characteristics. AJNR Am J Neuroradiol 2011;32:374–81.
33. Toh CH, Castillo M, Wong AM, Wei KC, Wong HF, Ng SH, Wan YL. Differentiation between classic and atypical meningiomas with use of diffusion tensor imaging. AJNR Am J Neuroradiol 2008;29:1630-5.
34. Filippi CG, Edgar MA, Uluğ AM, Prowda JC, Heier LA, Zimmerman RD. Appearance of meningiomas on diffusion-weighted images: correlating diffusion constants with histopathologic findings. AJNR Am J Neuroradiol 2001;22:65-72.
35. Homer J, Beevers M. Driven-equilibrium single-pulse observation of T1 relaxation. A re-evaluation of a rapid 'new' method for determining NMR spin-lattice relaxation times. J Magn Reson 1985;63:287–97.

36. Stikov N, Boudreau M, Levesque IR, Tardif CL, Barral JK, Pike GB. On the accuracy of T1 mapping: searching for common ground. Magn Reson Med 2015;73:514-22.
37. Byrnes T, Barrick T, Ladroue C, Bell B, Clark C. DTI and tractography metrics discriminate between brain tumour types in vivo. Proceedings from the International Society of Magnetic Resonance Medicine. 2006. p. 608.
38. Byrnes TJD, Barrick TR, Bell BA, Clark CA. Diffusion tensor imaging discriminates between glioblastoma and cerebral metastases in vivo. NMR Biomed 2011;24:54–60.

Legends

Figure 1: Maps of (a, b) T_2-weighted signal intensity, (c) magnetization transfer ratio (MTR; %), (d) longitudinal relaxation time (T_1; s), (e) mean ($\langle D \rangle$; $\times 10^{-6}$ mm^2/s), (f) axial (λ_{AX}; $\times 10^{-6}$ mm^2/s) and (g) radial (λ_{RAD}; $\times 10^{-6}$ mm^2/s) diffusivity, and (h) fractional anisotropy (FA) at the level of the lateral ventricles for a 47 year old male patient with a left hemisphere meningioma. Regions of tumor and edema are indicated in red and blue in (b). All images are displayed in radiological convention.

Figure 2: Maps of (a, b) T_2-weighted signal intensity, (c) magnetization transfer ratio (MTR; %), (d) longitudinal relaxation time (T_1; s), (e) mean ($\langle D \rangle$; $\times 10^{-6}$ mm^2/s), (f) axial (λ_{AX}; $\times 10^{-6}$ mm^2/s) and (g) radial (λ_{RAD}; $\times 10^{-6}$ mm^2/s) diffusivity, and (h) fractional anisotropy (FA) at the level of the lateral ventricles for a 33 year old female patient with a right hemisphere low-grade glioma. Regions of tumor and edema are indicated in red and blue in (b). All images are displayed in radiological convention.

Figure 3: Bar plots showing differences between meningioma and low-grade glioma (LGG) relative to contralateral normal-appearing white matter (NAWM) for both (a) tumor and (b) edema for magnetization transfer ratio (MTR), longitudinal relaxation time (T_1), mean ($\langle D \rangle$), axial (λ_{AX}) and radial (λ_{RAD}) diffusivity, and fractional anisotropy (FA). The asterisk indicates a significant difference between tumor types at the $p < 0.05$ level.

Table 1. Mean imaging biomarker values for meningioma and low-grade glioma (LGG).

	N	MTR (%)	T_1 (s)	$\langle D \rangle$ ($\times 10^{-6}$ mm^2/s)	λ_{AX} ($\times 10^{-6}$ mm^2/s)	λ_{RAD} ($\times 10^{-6}$ mm^2/s)	FA
Tumor							
Meningioma	9	43.67 ± 3.28*	1.62 ± 0.13*	856 ± 130*	1006 ± 149*	781 ± 123*	0.19 ± 0.04*
LGG	9	39.02 ± 4.04*	2.01 ± 0.45*	1367 ± 168*	1511 ± 166*	1294 ± 171*	0.11 ± 0.02*
p-value		< 0.02	0.02	<< 0.001	<< 0.001	<< 0.001	<< 0.001
Edema							
Meningioma	6	47.23 ± 4.16	1.31 ± 0.19*	1146 ± 152	1421 ± 140	1008 ± 159	0.24 ± 0.05*
LGG	6	45.36 ± 3.95	1.68 ± 0.35*	1216 ± 154	1391 ± 149	1129 ± 156	0.15 ± 0.02*
p-value		0.44	< 0.05	0.44	0.73	0.21	< 0.002
Ipsilateral normal-appearing white matter							
Meningioma	9	54.20 ± 2.98	1.06 ± 0.10	716 ± 37	920 ± 24	613 ± 48	0.28 ± 0.04
LGG	9	55.83 ± 0.79	1.08 ± 0.17	734 ± 61	926 ± 47	637 ± 69	0.26 ± 0.04
p-value		0.13	0.77	0.46	0.76	0.40	0.31
Contralateral normal-appearing white matter							
Meningioma	9	55.23 ± 2.23	1.01 ± 0.08	704 ± 39	901 ± 29	606 ± 49	0.27 ± 0.04
LGG	9	56.45 ± 0.68	1.06 ± 0.17	719 ± 57	909 ± 43	623 ± 65	0.26 ± 0.04
p-value		0.14	0.46	0.53	0.65	0.52	0.59

MTR = magnetization transfer ratio; T_1 = longitudinal relaxation time; $\langle D \rangle$ = mean diffusivity; λ_{AX} = axial diffusivity; λ_{RAD} = radial diffusivity; FA = fractional anisotropy. p-value given for difference between meningioma and LGG in each ROI. *indicates statistical significance ($p < 0.05$).

Table 2. Ratio of each biomarker value to contralateral normal-appearing white matter for meningioma and low-grade glioma (LGG).

	N	MTR	T_1	$\langle D \rangle$	λ_{AX}	λ_{RAD}	FA
Tumor							
Meningioma	9	0.79 ± 0.05*	1.61 ± 0.12*	1.22 ± 0.18*	1.12 ± 0.17*	1.29 ± 0.21*	0.71 ± 0.19*
LGG	9	0.69 ± 0.07*	1.91 ± 0.40*	1.92 ± 0.31*	1.67 ± 0.23*	2.10 ± 0.37*	0.43 ± 0.11*
p-value		0.002	< 0.05	<< 0.001	<< 0.001	<< 0.001	< 0.002
Edema							
Meningioma	6	0.86 ± 0.051	1.36 ± 0.22*	1.64 ± 0.26	1.56 ± 0.16	1.70 ± 0.34	0.90 ± 0.31*
LGG	6	0.80 ± 0.067	1.62 ± 0.37*	1.72 ± 0.02	1.55 ± 0.18	1.85 ± 0.28	0.58 ± 0.09*
p-value		0.088	<< 0.001	0.56	0.95	0.43	< 0.05
Ipsilateral normal-appearing white matter							
Meningioma	9	0.98 ± 0.02	1.05 ± 0.07	1.02 ± 0.03	1.02 ± 0.03	1.01 ± 0.04	1.04 ± 0.09
LGG	9	0.99 ± 0.01	1.02 ± 0.03	1.02 ± 0.03	1.02 ± 0.02	1.02 ± 0.03	1.00 ± 0.03
p-value		0.32	0.24	0.79	0.77	0.60	0.22

MTR = magnetization transfer ratio; T_1 = longitudinal relaxation time; $\langle D \rangle$ = mean diffusivity; λ_{AX} = axial diffusivity; λ_{RAD} = radial diffusivity; FA = fractional anisotropy. p-value given for difference between meningioma and LGG in each ROI. *indicates statistical significance ($p < 0.05$).

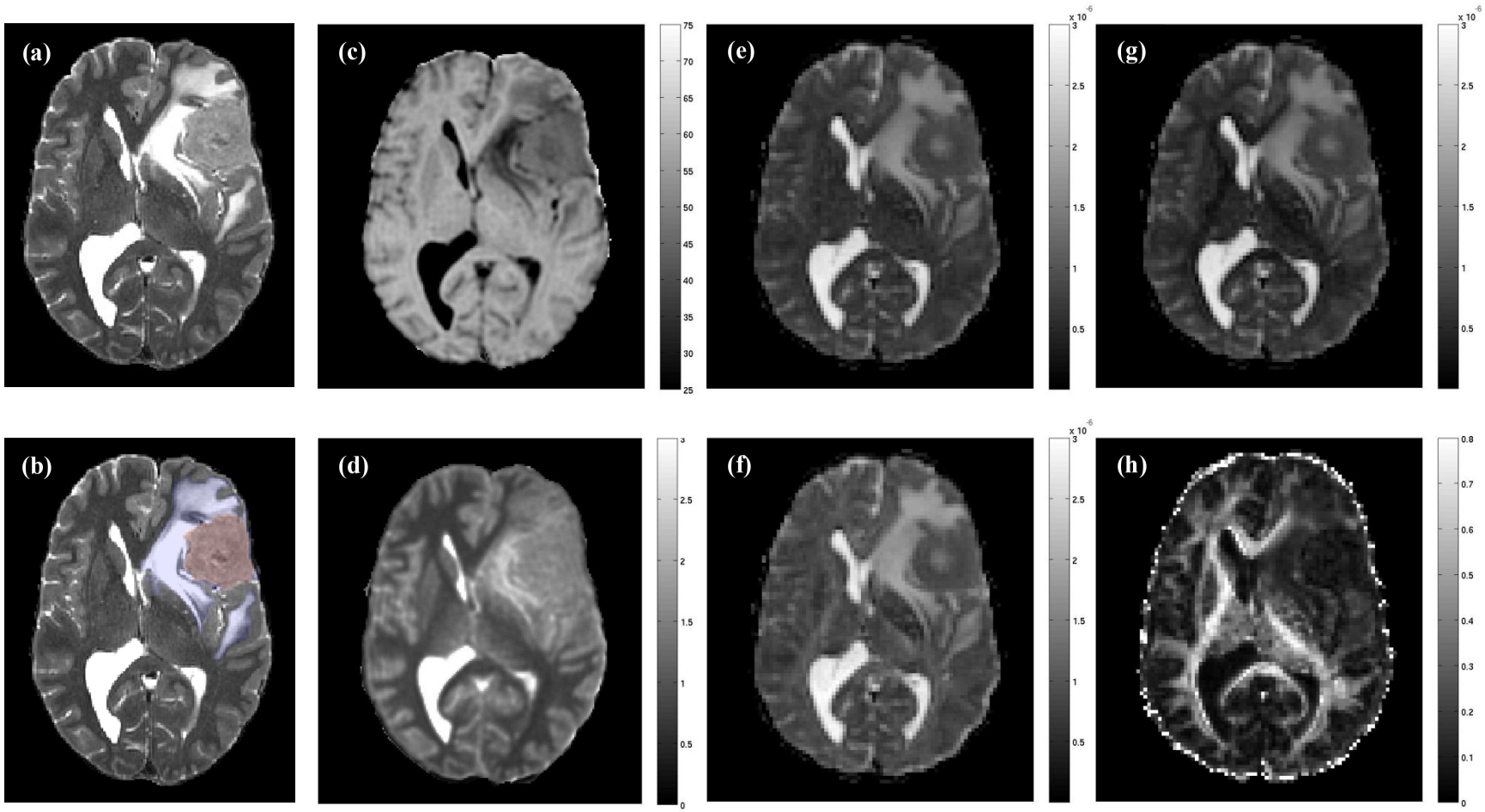

Figure 1

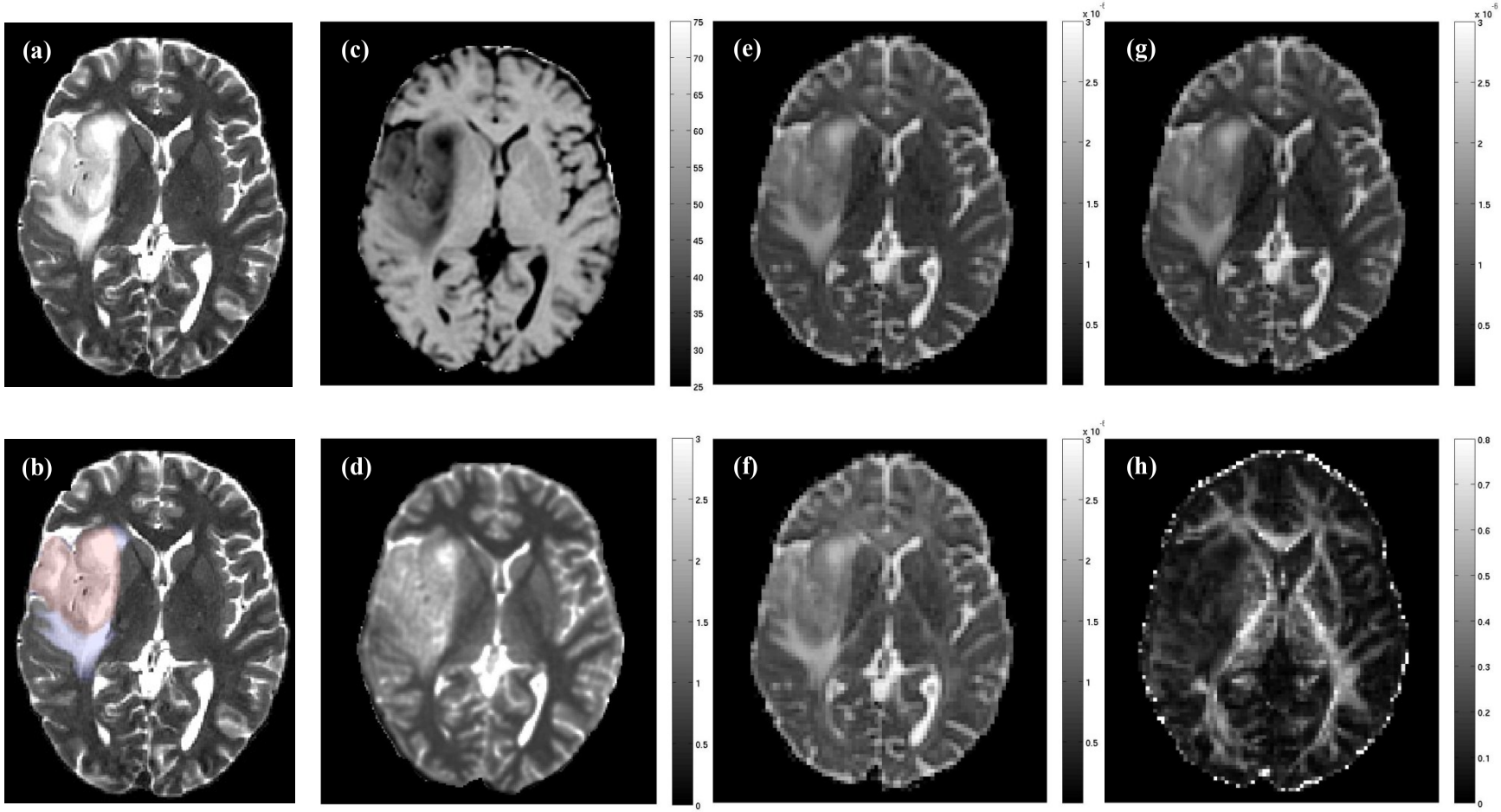

Figure 2

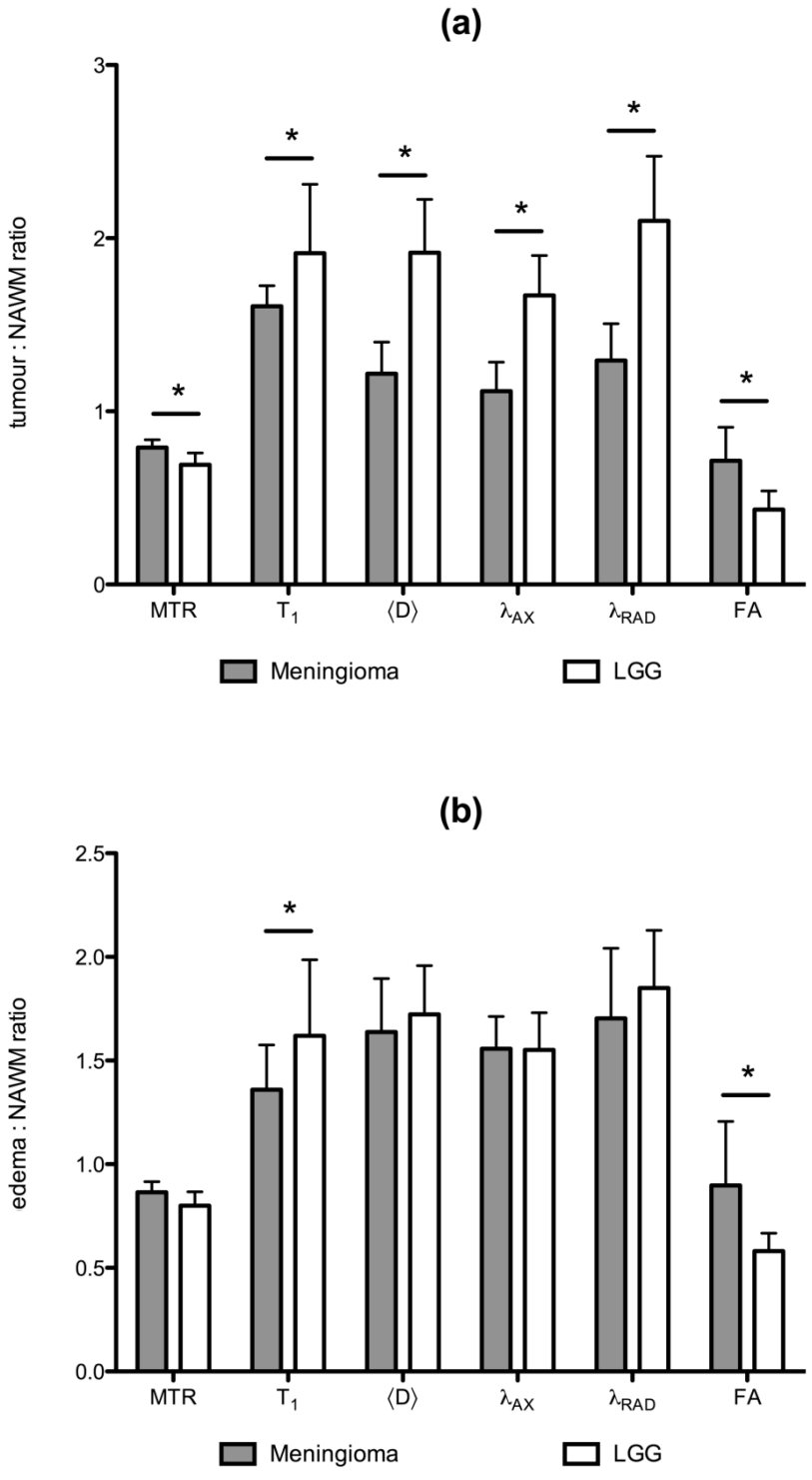
(a)
tumour : NAWM ratio
3
2
1
0
*
MTR
T1
⟨D⟩
λAX
λRAD
FA
Meningioma
LGG
(b)
edema : NAWM ratio
2.5
2.0
1.5
1.0
0.5
0.0
MTR
T1
⟨D⟩
λAX
λRAD
FA
Meningioma
LGG

Figure 3